HHS Public Access

Author manuscript

Biochem J. Author manuscript; available in PMC 2021 October 30.

Published in final edited form as:

Biochem J. 2020 October 30; 477(20): 4053–4070. doi:10.1042/BCJ20200695.

Comparison of tyrosine kinase domain properties for the neurotrophin receptors TrkA and TrkB

Stephen C. Artim[*,†,¶], **Anatoly Kiyatkin**[*,§], **Mark A. Lemmon**[*,†,§]

[*]Department of Biochemistry and Biophysics, University of Pennsylvania Perelman School of Medicine, Philadelphia, PA 19104, USA

[†]Graduate Group in Biochemistry and Molecular Biophysics, University of Pennsylvania Perelman School of Medicine, Philadelphia, PA 19104, USA

[¶]Present address: Merck Research Laboratories, Merck, South San Francisco, CA 94080, USA

[§]Department of Pharmacology and Cancer Biology Institute, Yale University School of Medicine, New Haven, CT, 06520, USA

Abstract

The tropomyosin-related kinase (Trk) family consists of three receptor tyrosine kinases (RTKs) called TrkA, TrkB, and TrkC. These RTKs are regulated by the neurotrophins, a class of secreted growth factors responsible for the development and function of neurons. The Trks share a high degree of homology and utilize overlapping signaling pathways, yet their signaling is associated with starkly different outcomes in certain cancers. For example, in neuroblastoma, TrkA expression and signaling correlates with a favorable prognosis, whereas TrkB is associated with poor prognoses. To begin to understand how activation of the different Trks can lead to such distinct cellular outcomes, we investigated differences in kinase activity and duration of autophosphorylation for the TrkA and TrkB tyrosine kinase domains (TKDs). We find that the TrkA TKD has a catalytic efficiency that is ~2-fold higher than that of TrkB, and becomes autophosphorylated *in vitro* more rapidly than the TrkB TKD. Studies with mutated TKD variants suggest that a crystallographic dimer seen in many TrkA (but not TrkB) TKD crystal structures, which involves the kinase-insert domain, may contribute to this enhanced TrkA autophosphorylation. Consistent with previous studies showing that cellular context determines whether TrkB signaling is sustained (promoting differentiation) or transient (promoting proliferation), we also find that TrkB signaling can be made more transient in PC12 cells by suppressing levels of $p75^{NTR}$. Our findings shed new light on potential differences between TrkA and TrkB signaling, and suggest that subtle differences in signaling dynamics can lead to substantial shifts in cellular outcome.

Correspondence to: Mark A. Lemmon, Yale Cancer Biology Institute, Advanced Biosciences Center (ABC) 301, 840 West Campus Drive, PO Box 27400, West Haven, CT 06516, USA, Tel: (203) 737-7360, mark.lemmon@yale.edu.

AUTHOR CONTRIBUTIONS

S.C.A. performed all experimental work with TKDs, and A.K. performed cell signaling studies. S.C.A. and M.A.L. interpreted results and prepared the manuscript with input from A.K.. All authors contributed to editing the manuscript.

COMPETING FINANCIAL INTERESTS

The authors declare no competing financial interests.

DATA AVAILABILITY STATEMENT

All data required to evaluate the work are included in the manuscript, and are available on request.

Keywords

receptor tyrosine kinase (RTK); TrkA; TrkB; neurotrophin; autophosphorylation; kinase insert domain

INTRODUCTION

The tropomyosin receptor kinase (Trk) family [1] comprises three receptor tyrosine kinases (RTKs) called TrkA, TrkB, and TrkC that are activated by neurotrophins. TrkA functions as the primary receptor for nerve growth factor (NGF), TrkB is the primary receptor for brain-derived neurotrophic factor (BDNF) and neurotrophin-4 (NT-4), and TrkC is the primary receptor for neurotrophin-3 (NT-3). The Trks primarily regulate neuronal survival and differentiation through a highly complex set of tightly controlled cell-specific and receptor-specific interactions. In addition, they are associated with certain cancers, notably neuroblastoma, where the different receptors play starkly different roles [2, 3]. Activating TrkA and TrkB in the same cell type can yield very different cellular outcomes. For example, activating TrkA signaling in neuroblastoma cells inhibits cell growth, whereas activation of TrkB does not [4]. Indeed, whereas TrkA expression and activation promotes cell differentiation and a favorable prognosis in neuroblastoma, TrkB expression and activation conversely causes cell proliferation and is associated with a poor prognosis [2, 3, 5, 6]. TrkA and TrkB are 49% identical overall, with >76% sequence identity in the intracellular region. How can two homologous RTKs, both thought to engage similar downstream signaling pathways, produce opposite cellular responses?

Despite their association with favorable and unfavorable outcome respectively in neuroblastoma, studies of global gene regulation following ligand stimulation in engineered neuroblastoma cells have suggested a surprising degree of similarity, apart from differential expression of a few target genes [7]. This raises the possibility that differences in kinetics or time course of signaling – rather than pathways – may be the primary determinant of cellular outcome. Now-classic studies in rat pheochromocytoma (PC12) cells [8, 9] showed that duration of extracellular regulated kinase (ERK) signaling downstream of RTKs defines the nature of the response. NGF activates TrkA to promote sustained signaling and differentiation, whereas activation of EGFR with EGF leads to transient signaling and proliferation. These different cell fates arise in part from phosphorylation-dependent regulation of immediate-early gene product stability [10]. Recent studies argue that the dynamics of ERK signaling downstream of an RTK are substantially defined at the level of receptor activation kinetics [11–14]. Moreover, we and others have shown that the same intracellular tyrosine kinase domain (from EGFR) can signal with different kinetics and cellular outcome depending on how it is activated [14–18].

The different prognoses associated with TrkA and TrkB signaling in neuroblastoma [2, 3] and certain other cancers [19, 20] suggest the possibility of intrinsic signaling differences between the two receptors. So do differences in response to optogenetically activated TrkA and TrkB kinase domains that have been reported in Xenopus embryos [21]. Motivated by these observations, we initiated an investigation of possible differences in kinase activity

between the TrkA and TrkB tyrosine kinase domains (TKDs). Through *in vitro* kinase and autophosphorylation assays, we characterize the effects of autophosphorylation on TKD activation for TrkA and TrkB. We find that they are quite similar kinetically, but TrkA does have a slightly – but significantly – higher catalytic efficiency than TrkB when fully active. Moreover. TrkA undergoes more efficient autophosphorylation than TrkB *in vitro*, which may be enhanced by crystallographically observed TrkA-specific interactions involving its unique kinase insert domain (KID). Finally, motivated by studies of the effects of the low affinity neurotrophin receptor $p75^{NTR}$ on neuroblastoma [22, 23], we found that siRNA knockdown of this receptor makes TrkB signaling more transient when exogenously expressed in PC12 cells. These data, and others [24] suggest that the kinetic characteristics of TrkB signaling, and its association with proliferation or differentiation depend on the expression of co-receptors and other molecules that influence its signaling networks. Our results have implications for Trk receptor targeting in neuroblastoma and other settings, focusing attention on the kinetics of their signaling.

MATERIALS AND METHODS

Plasmid Construction

Sequence and structure alignments facilitated the design of analogous TrkA TKD and TrkB TKD constructs used for protein expression. DNA encoding intracellular domain residues 498–796 of human TrkA (NCBI reference sequence NM_002529.3) and residues 526–822 of human TrkB (NCBI reference sequence NM_001018064.3) were amplified by PCR, also adding a sequence encoding an N-terminal hexahistidine tag and unique *EcoRI* and *XhoI* restriction sites for subcloning. The $TrkA^{B\text{-}KID}$ TKD variant, with its kinase insert domain (KID) engineered to resemble that of TrkB was generated by introducing the following mutations into TrkA TKD: $Glu^{615}Asn$, Asp^{616}_Val^{617}del, $Ala^{618}Pro$. *EcoRI*/*XhoI* digested PCR fragments were subcloned into pFastBac1 (Invitrogen) cut with the same restriction enzymes. The Bac-to-Bac expression system (Invitrogen) was then used for generation of recombinant baculoviruses and for protein expression in *Spodoptera frugiperda* Sf9 cells.

Production and Purification of Proteins

TrkA, TrkB, or mutated $TrkA^{B\text{-}KID}$ TKDs were produced as previously described for the TrkA TKD [25]. Sf9 cell lysate was mixed with Ni-NTA beads (Qiagen) for 1 h at 4°C. Beads were washed in 50 column-volumes of lysis buffer: 50 mM KH_2PO_4/Na_2HPO_4, pH 8.0, containing 300 mM NaCl, 5% w/v glycerol, 10 mM imidazole, 10 mM 2-mercaptoethanol, 0.5 mM PMSF, and Roche protease inhibitor cocktail. The bound TKD was eluted with increasing concentrations of imidazole in the same buffer, and was further purified using a Fractogel SO_3^- cation exchange column (EMD) in 25 mM MES, pH 6, containing 5% glycerol, 2 mM DTT (eluting with a gradient from 10 mM to 1 M NaCl). The TKD proteins were concentrated to 5–6 ml by ultrafiltration, and were then treated with 2 μM YopH phosphatase for 1 h at 30°C in the presence of 1mM EDTA. YopH was purified away by repeating the cation exchange step. Trk TKDs were then concentrated again to 5–6 ml and treated with 2 μM λ phosphatase in the presence of 5 mM $MnCl_2$ for 1 h at 30°C, with subsequent removal of λ phosphatase using a cation exchange step. The TKDs were next applied to a HiTrap Butyl Sepharose HP column (GE Healthcare) in 25 mM MES, pH

6.0, containing 150 mM NaCl and 2 mM DTT, and were eluted with a gradient from 0.8 M to 0 M $(NH_4)_2SO_4$. The final purification step was size exclusion chromatography using a 10/300 Superdex 200 column (GE Healthcare) equilibrated in 25 mM HEPES, pH 8.0, containing 150 mM NaCl and 2 mM DTT. Apparent T_m values from thermal melts monitored by circular dichroism for both the TrkA and TrkB TKDs were above 37°C (Fig. S1), indicating that these proteins are stable under the experimental conditions used in this study. Sedimentation equilibrium analytical ultracentrifugation experiments (SE-AUC) were also performed to ensure that the TrkA and TrkB TKD proteins do not aggregate detectably (Fig. S2).

YopH BL21 cells were grown in 1 liter of LB with 50 μg/ml streptomycin at 37°C until a density of ~0.6 OD(600) was reached. The cultures were then cooled to 18°C and subsequently induced with 1 mM isopropyl β-D-1-thiogalactopyranoside (IPTG) overnight. Cells were harvested by centrifugation at 2,000 × g for 15 min at 4°C and lysed by sonication in 50 mM HEPES, pH 7.4, 300 mM NaCl, 10% glycerol, 10 mM imidazole, 10 mM 2-mercaptoethanol, 0.5 mM PMSF and protease inhibitor cocktail (Roche). The lysate was incubated with Ni-NTA beads (Qiagen) for 1 h at 4°C, and beads washed with 20 mM imidazole prior to eluting YopH with 300 mM imidazole. YopH was then loaded onto a Fractogel SO_3^- cation exchange column (EMD) equilibrated with 25 mM MES, pH 6, containing 5% glycerol, 2 mM DTT and eluted using a gradient from 10 mM to 1 M NaCl. Fractions containing YopH were pooled, concentrated and loaded onto a 10/300 Superdex 200 column (GE Healthcare) equilibrated in 25 mM MES, pH 6, containing 250 mM NaCl and 2 mM DTT.

λ phosphatase was expressed in *E. coli* and purified essentially as described [26]. Cell lysate was loaded onto a phenylsepharose column and peak fractions were pooled, concentrated and loaded onto a 10/300 Superdex 200 size exclusion column (GE Healthcare) equilibrated in 25 mM Tris, pH 7.5, containing 150 mM NaCl. Purified λ phosphatase was stored at −80°C at 20 mg/ml in 25 mM Tris, pH 7.5, 150 mM NaCl, plus 10% w/v glycerol.

Autophosphorylation Assays

All autophosphorylation reactions were conducted in the presence of 1 mM ATP (Sigma-Aldrich) and 10 mM $MgCl_2$ in a buffer containing 100 mM HEPES pH 7.4, 150 mM NaCl, 2 mM DTT and 1x Halt phosphatase inhibitor cocktail (Thermo Scientific #1862495), which contains sodium fluoride, sodium orthovanadate, sodium pyrophosphate, and β-glycerophosphate. Figure legends indicate the concentrations of TrkA and TrkB TKD proteins used for autophosphorylation reactions, ranging from 1 to 10 μM, and also indicate the temperature at which reactions were incubated (ranging from 15°C-37°C). Autophosphorylation reactions were analyzed by different gel-based methods including SDS-PAGE autoradiography, SDS-PAGE Western blotting, and Phos-Tag SDS-PAGE. For SDS-PAGE autoradiography, gels were dried and imaged using a PhoshorImager, and normalized using the near infrared fluorescence signal from protein-bound Coomassie blue stain from the same gel using ImageStudio software (LI-COR Biosciences).

Generation and purification of phospho-Trk TKD

Autophosphorylation reactions were conducted to generate phospho-Trk (pTrk) TKDs for kinetic studies. Western blotting of Phos-Tag gels with phosphospecific antibodies was used to monitor the reactions and ensure phosphorylation was as close to stoichiometric as possible, with examples shown in Fig. S3. TrkA TKD at 10 μM was incubated at room temperature with 1 mM ATP, 10 mM $MgCl_2$ in 100 mM HEPES pH 7.4, 150 mM NaCl, containing 2 mM DTT. After 5 min, the reaction was quenched with EDTA (final concentration of 100 mM) – at which time no detectable unphosphorylated protein remained and the pTrkA TKD reacted with antibodies to $pTyr^{676}$, $pTyr/pTyr^{680/681}$ and $pTyr^{791}$ (see below). For TrkB-TKD, 7.5 μM protein was incubated at 30°C with 1 mM ATP, 10 mM $MgCl_2$ in 100 mM HEPES pH 7.4, 150 mM NaCl, 2 mM DTT and 1x Halt phosphatase inhibitor cocktail, and the reaction was quenched after 4 min with 100 mM EDTA, based on Phos-Tag gels as shown in Fig. S3 and Western blotting with phospho-specific antibodies. Samples were filtered and loaded onto a 10/300 Superdex 200 column (GE Healthcare) equilibrated in 25 mM HEPES, pH 8, 150 mM NaCl, 2 mM DTT, containing 1x Halt phosphatase inhibitor cocktail to remove EDTA prior to kinetic analysis.

Quantitative kinase assays to measure k_{cat} and K_m values

Quantitative kinase assays monitored incorporation of ^{32}P-labeled phosphate into peptide mimics of the TrkA and TrkB activation loop (SRDIYSTDYYRVGGRTMLPIR for TrkA and (SRDVYSTDYYRVGGHTMLPIR for TrkB), purchased from CanPeptide. Reactions were performed at room temperature (RT) in 100 mM HEPES pH 7.4, 150 mM NaCl, 0.5 mg/ml BSA, 2 mM DTT, 10 mM $MgCl_2$, 1x Halt phosphatase inhibitor cocktail and trace amounts of $\gamma-^{32}P$ ATP (20–40 μCi). For $K_{m,\ ATP}$ determination, TrkA and TrkB TKDs were assayed with various ATP concentrations (0.039 mM to 5 mM) with 10 mM $MgCl_2$ and peptide substrate at a fixed concentration of 2 mM. For $K_{m,\ peptide}$ determination, TrkA and TrkB TKDs were assayed with various peptide concentrations (0.031 mM to 4 mM), 10 mM $MgCl_2$ and a fixed ATP concentration of 2 mM. Protein concentrations were 30 nM for dephosphorylated TrkA TKD, 400 nM for dephosphorylated TrkB TKD, and 8 nM for both phosphorylated TrkA and phosphorylated TrkB TKDs. Values for k_{cat} were determined from rates when both substrates were saturating in the K_m determination experiments.

Reaction progress was monitored essentially as described [27]. Samples were taken at each time point from the reactions listed above, spotted onto squares of P81 phosphocellulose paper (Millipore # 20–134), and immediately quenched with 0.5% phosphoric acid. The phosphocellulose squares were then washed extensively with 0.5% phosphoric acid and dried with acetone. Incorporated radioactivity was then measured for each phosphocellulose square by scintillation counting using a Tri-Carb 2900TR liquid scintillation analyzer (PerkinElmer). Initial rates were determined under conditions of <10% product formation – ensuring linearity. These rates were converted to specific activity, normalized for enzyme concentration, and data were fit to the Michaelis-Menten equation ($v_o = v_{max}[S]/(K_m+[S])$) using GraphPad Prism version 8.4.2. Unpaired two-tailed *t*-tests were used to determine statistical significance of differences in enzymatic parameters between TrkA TKD and TrkB TKD in Table 1.

Radioactive autophosphorylation assays

Parallel radioactive autophosphorylation assays were performed at RT with 4 μM of TrkA TKD, $TrkA^{B\text{-}KID}$, or TrkB TKD protein in the presence of 2 mM ATP, 10 mM $MgCl_2$ 100 mM HEPES pH 7.4, 150 mM NaCl, 2 mM DTT, 1x Halt phosphatase inhibitor cocktail and trace amounts of γ–^{32}P ATP (40 μCi), but no peptide substrate. Samples taken at each time point were processed as above for the quantitative kinase assay samples. Counts from the scintillation analyzer were converted to moles of phosphate incorporated using measured γ–^{32}P-ATP specific activity and then normalized to enzyme concentration. Each reaction data set was converted to percent maximum moles of phosphate incorporated normalized to enzyme concentration.

Western Blotting

For SDS PAGE Western blotting, samples were separated on a 12.5% Laemmli gel, transferred to nitrocellulose and then blocked with blocking buffer (LI-COR Biosciences). Membranes incubated with primary antibody diluted in blocking buffer overnight at 4°C, washed with PBS containing 1% Tween-20, and then incubated with secondary antibody diluted in blocking buffer. Membranes were washed with PBS containing 1% Tween-20 and then subjected to a final wash with just PBS. Membranes were imaged using the Odyssey® FC (LI-COR Biosciences) imaging station.

Phos-Tag gels were made using the Phos-Tag acrylamide reagent (Wako Pure Chemical Industries, Ltd., catalog # AAL-107) along with $ZnCl_2$ as previously described [28]. The composition of reagents for optimal separation of phosphorylated Trk TKD species was 25 μM Phos-Tag acrylamide reagent and a 10% acrylamide gel using acrylamide:bis solution (29:1). Gels were run at a constant 70V for 3 hours. Phos-Tag gels were stained at room temperature for 15–20 min with Coomassie brilliant blue R-250. For Western blotting, prior to transferring to nitrocellulose, Phos-Tag gels were soaked in transfer buffer containing 1 mM EDTA for 15 min and then washed for 15 min in transfer buffer without EDTA. The rest of the Western blot protocol was performed as described above.

For Western blotting, the goat pan-Trk antibody (Santa Cruz: sc-11-g) and rabbit pTrkA $pTyr^{676}$ (Santa Cruz: sc-130222) antibodies were used at a 1:500 dilution. The rabbit pTrkA $pTyr/pTyr^{680/681}$ (Cell Signaling Technology/CST# 4621) and rabbit pTrkA $pTyr^{791}$ (CST# 4168) were used at 1:1000 dilution. Note that the Cell Signaling pTrk antibodies are sold using the TrkA isoform *I* numbering, thus pTyr-pTyr/$pTyr^{674/675}$ and $pTyr^{785}$ corresponds to $pTyr/pTyr^{680/681}$ and $pTyr^{791}$ in isoform *II*, respectively, and also bind to the corresponding TrkB phosphotyrosines. The specificity of these antibodies has previously been tested with mutagenesis and peptide competition assays [29, 30]. Secondary antibodies used were IRDye® 800CW donkey anti-rabbit IgG (LI-COR Biosciences: 926–32213) and IRDye® 680RD donkey anti-goat IgG (LI-COR Biosciences : 926–68074).

For the SDS PAGE Western blots, each phosphospecific signal was normalized for total Trk. Normalized signal from a phosphospecific antibody was then expressed as a fraction of the maximum signal seen with that antibody for TrkA or TrkB TKD autophosphorylation

respectively. Using these data, the normalized relative signals for each phosphospecific antibody could be compared directly between sites and TKDs.

Structure visualization and alignment

Structure figures and alignments were generated using PyMOL (The PyMOL Molecular Graphics System, Version 2.0.7, Schrödinger, LLC). All structures were aligned to our previously determined inactive TrkA structure (PDB code 4GT5).

Studies of Trk signaling in PC12 cells

PC12 cells and/or PC12 cells stably expressing TrkB (TrkB-PC12) were cultured at 37°C, humidified 5% CO_2 in complete RPMI-1640 medium containing L-glutamine and HEPES (ThermoFisher Sci #22400089), supplemented with 1 mM sodium pyruvate (ThermoFisher Sci #11360070), 5% fetal bovine serum (FBS) (Atlanta Biologicals #S11550), 10% heat inactivated horse serum (ThermoFisher Sci #26050088) as well as 100 U/ml penicillin and 100 μg/ml streptomycin (ThermoFisher Sci #15140122). To subculture, harvested cells were centrifuged at 200 × *g* for 10 min, supernatant removed and the cell pellet was resuspended in fresh medium. Cell culture was aspirated several times with a syringe outfitted with a 22-gauge needle to break up cell clusters. Aliquots of cell suspension then were added to new T-75 flasks containing 10–15 ml fresh medium and cells were cultured up to cell density 2–4 × 10^6 cells/ml.

Generation of TrkB-PC12 stable cell line: A cDNA construct directing expression of full length human TrkB was transfected into PC12 cells using electroporation with Nucleofector 2b device as described below for siRNA procedure. Transfected cells were selected for 2 weeks in medium containing 0.5 mg/ml G418. Stable clones were maintained in the presence of 250 mg/ml G418. TrkB expression levels were confirmed by Western blotting using anti-TrkB antibody (CST #4603).

Transient cell transfection with siRNA: TrkB-PC12 or parental PC12 cells were harvested and aspirated several times with a syringe outfitted with a 22-gauge needle to break up cell clusters. 2 × 10^6 cells per sample were aliquoted into Eppendorf tubes and centrifuged at 100 × *g* for 10 min. The cell pellet was resuspended in 100 μl of Ingenio transfection solution (Mirus #MIR50111) containing siRNA. 100 nM of rat specific SMARTpool siGENOME $p75^{NTR}$ siRNA (Dharmacon # M-080041-01-0005) was used to compare cell responses to those transfected with 100 nM AllStars Negative Control siRNA (Qiagen #1027280). Cell suspensions containing siRNA were electroporated using the U-029 program on Nucleofector 2b device (Lonza, Basel, Switzerland). The pre-equilibrated antibiotic-free complete medium was added to the cuvette immediately after electroporation and transferred into 60 × 15 mm Corning BioCoat collagen I-coated dishes (Fisher Sci #356401) to a final volume of 2 ml. Penicillin-streptomycin solution was added to the cells after 6 h. On the next day, cell culture medium was replaced with 5 ml of fresh complete medium. Cell signaling experiments were performed 72 h post-transfection.

Cell stimulation: parental PC12 cells and/or TrkB-PC12 were harvested from T-75 flasks, centrifuged and subjected to the needle aspiration procedure described above. Cells were

seeded on 100 × 20 mm Corning BioCoat collagen I-coated dishes (Fisher Sci #356450) in complete growth medium at a density of 1×10^6 cells/ml (10 ml per dish) and grown for one day at 37°C in 5% CO_2. Before stimulation with ligands, cells were starved overnight in RPMI-1640 medium containing L-glutamine, HEPES, sodium pyruvate and penicillin-streptomycin. PC12 or TrkB-PC12 cells transiently transfected with siRNA $p75^{NTR}$ or control siRNA for 72 hours were left unstimulated or were stimulated with 50 ng/ml BDNF (R&D Systems #248-BD reconstituted in PBS with 1 mg/ml BSA) or 50 ng/ml rat NGF from R&D Systems (#556-NG-100) for the time intervals shown at 37°C in humidified 5% CO_2. Cells were lysed using ice-cold Cell Lysis Buffer (CST #9803) supplemented with Phosphatase Inhibitor Cocktail Tablets PhosSTOP (Roche #04906837001) and Protease Inhibitor Cocktail Tablets Complete (Roche #11697498001). Cells were scraped from the surface, harvested, vortexed, incubated for 30 min on ice, and then centrifuged at 10,000 × g for 10 min at 4°C. Aliquots of supernatant were dissolved in NuPAGE LDS sample buffer (ThermoFisher Sci #NP0007) supplemented with 50 mM DTT and heated for 7 min at 75°C.

Quantitative immunoblotting: Cell lysates were subjected to SDS-PAGE using NuPAGE™ Novex™ 4–12% Bis-Tris Protein Gels (ThermoFisher Sci #NP0321BOX). Separated proteins were electrotransferred onto nitrocellulose membranes (Bio-Rad #162–0112). The membranes previously blocked in 4% BSA solution were probed with the following primary antibodies. For assessment of pTrkB and pTrkA, a mixture of rabbit pTrkA pTyr/$pTyr^{680/681}$ (CST# 4621) and rabbit pTrkA $pTyr^{791}$ (CST #4168), described above, was used at 1:1000 dilution – recognizing pTyr/$pTyr^{706/707}$ and $pTyr^{817}$ respectively in human TrkB. For phospho-p44/42 MAPK (ERK1/2) ($pThr^{202}$/$pTyr^{204}$) (E10) (CST #9106) was used, for $p75^{NTR}$ (D4B3) XP Rabbit mAb (CST #8238), and for Grb2 (C-23) (Santa Cruz #sc-255) or Grb2 (CST #3972). Membranes were incubated with the corresponding secondary antibodies, either Horse Anti-Mouse IgG, HRP-linked Antibody (CST #7076) or Goat Anti-Rabbit IgG (H+L) Cross Adsorbed Secondary HRP conjugate (ThermoFisher Sci #31462) at 1:10,000 dilutions. Signals were detected by enhanced chemiluminescence system using SuperSignal West Pico Chemiluminescent Substrate (ThermoFisher Sci #34080). Bands were visualized and quantified with densitometry analysis using a KODAK Image Station 440CF (Kodak Scientific Imaging Systems, New Haven, CT). Signal intensities for a given protein were normalized by signal intensities of the loading control (Grb2 protein from the same gel) at each time point as described [14, 15]. Time courses of protein phosphorylation from different experiments were also compared by normalizing peak values at 5 min stimulation and were expressed in percent maximum.

RESULTS AND DISCUSSION

Quantitation of TrkA and TrkB kinase activity and effects of autophosphorylation

To explore possible differences between TrkA and TrkB, we first compared the activities of their intracellular tyrosine kinase domains (TKDs) in both the dephosphorylated (unactivated) and fully phosphorylated states. TrkA and TrkB contain five primary autophosphorylation sites [31–33]. Three are in the activation loop as part of the YxxxYY motif. Another lies in the juxtamembrane (JM) region (Tyr^{496} in TrkA, Tyr^{516} in TrkB) and

was removed in our constructs to optimize protein production levels. The fifth lies in the C-terminal tail (Tyr^{791} in TrkA, Tyr^{817} in TrkB), which is intact in the proteins used here. We fully dephosphorylated the purified TKDs by serial treatment with the YopH and λ phosphatases as described in Materials and Methods. To generate maximally phosphorylated proteins, autophosphorylation was allowed to proceed as described below (see also Materials and Methods), and the reaction was quenched at a time determined to correspond to its peak. We then monitored activity of the dephosphorylated and phosphorylated TKDs by following incorporation of ^{32}P from ^{32}P-γ-ATP into peptides that mimic the activation loop of either TrkA or TrkB (see Materials and Methods). Fig. 1 shows representative data used to obtain the kinetic parameters, and Table 1 lists kinetic parameters measured (and errors) for TrkA and TrkB TKDs in these assays.

The kinase activities of the TrkA and TrkB TKDs were very similar. Values for k_{cat} were slightly (10–30%) higher for TrkA than for TrkB in experiments with both phosphorylated and dephosphorylated protein, but these differences were not statistically significant across multiple repeats when subjected to Mann-Whitney-Wilcoxon tests. Similarly, $K_{m,\ ATP}$ values were slightly lower for TrkA than TrkB in both sets of experiments (Table 1), but this comparison alone did not reach statistical significance. The results did suggest a small but statistically significant difference in catalytic efficiency ($k_{cat}/K_{m,ATP}$) for the phosphorylated Trk TKDs, however, with the value for pTrkA being approximately 1.7-fold greater than that for pTrkB (P = 0.036 from a Mann-Whitney-Wilcoxon test, or 0.0005 from a Student's t-test).

As expected, autophosphorylation led to a dramatic increase in kinase activity for both TrkA TKD and TrkB TKD, with 70-fold and 85-fold increases in k_{cat} respectively. Autophosphorylation also reduced K_m values for ATP by ~10-fold, and for peptide by 3–5 fold Table 1). All phosphorylation-dependent changes in Table 1 were statistically significant. These changes upon phosphorylation are typical for tyrosine kinases in the insulin receptor family. Indeed, TKDs from the insulin receptor (IRK), IGF1 receptor, and MuSK have been reported to show phosphorylation-dependent increases in k_{cat} of between 20 and 230-fold, with associated 6–10-fold reductions in K_m for ATP and peptide [34–37]. The IRK, IGF1-R and MuSK TKDs are the closest homologues of the Trk TKDs. All share >40% sequence identity and adopt very closely related conformations in their inactive states [25]. Like TrkA and TrkB, the IGF1-R and MuSK TKDs share a characteristic mode of peptide binding site occlusion by the second tyrosine of the YxxxYY motif first seen in IRK [38], and of ATP-binding site occlusion by the remainder of the activation loop. Interestingly, TKDs that contain an activation loop YxxxYY motif but do not adopt the IRK-like autoinhibitory conformation, namely c-Met and ALK [25], show smaller changes in K_m upon autophosphorylation. In the case of c-Met, K_m for peptide is reduced by only ~1.5-fold by autophosphorylation, and $K_{m,ATP}$ by ~5-fold [39]. More notably, autophosphorylation of ALK changes K_m for peptide by less than 2-fold, and actually increases (rather than decreases) $K_{m,ATP}$ [27]. These differences in the effects of activation loop autophosphorylation provide evidence for the altered modes of (or lack of) of ATP-binding site occlusion in the unique autoinhibitory conformations seen for c-Met and ALK (and Ron) in this tyrosine kinase family.

Autophosphorylation and dephosphorylation of TrkA and TrkB TKDs

In the course of optimizing autophosphorylation of the TrkA and TrkB TKDs for these experiments, we found by monitoring ^{32}P incorporation that TrkA-TKD becomes autophosphorylated more rapidly than TrkB-TKD when analyzed at the same concentration (10 μM) under the same conditions (Fig. S4). This is a protein concentration that mimics a receptor density of ~10^5 receptors per cell [40, 41], so is likely to be relevant for events at the cell surface. TrkA-TKD autophosphorylation peaked at approximately 1 min at 37°C (Fig. S4A,B), whereas TrkB-TKD autophosphorylation peaked at ~2.5 min, effectively displaying a lag phase at the beginning of the reaction – as reported in earlier studies of the TrkB intracellular region [42]. This difference was maintained, but spread out in time, in studies at room temperature (Fig. S4C,D), with TrkA autophosphorylation peaking at around 5 min and TrkB at 10 min, with a longer lag phase than seen at 37°C. Interestingly, once autophosphorylation had reached its peak, the ^{32}P signal was progressively lost over time, indicating dephosphorylation of the purified TKDs. This is particularly noticeable in the autoradiograms shown for TrkA and TrkB TKDs in Fig. S4A. Similar dephosphorylation has been reported for IRK [43–46], where it was shown to be ADP dependent, to coincide with transfer of ^{32}P-phosphate from IRK into ATP [45], and to be inhibited by EDTA or staurosporine [43, 46]. Similar phenomena have also been observed for the IGF1-R TKD [37] and the fibroblast growth factor (FGF) receptor-1 [47]. Moreover, the vascular endothelial growth factor (VEGF) receptor-2 was shown to be capable of catalyzing transfer of phosphate from a peptide substrate to Mg^{2+}-ADP [48], albeit with a k_{cat} of just 0.1 s^{-1}. We tried to identify contaminating protein tyrosine phosphatases in our Trk TKD preparations using mass spectrometry – but found none. As in the earlier IRK studies, we also could not arrest Trk TKD dephosphorylation with phosphatase inhibitors (data not shown). Thus, the Trk TKDs appear to share this feature with other IRK-family kinases. Interestingly, the auto-dephosphorylation seen here was not observed in our extensive studies of the ALK TKD [27], and was not evident in detailed studies of the c-Met TKD [39]. Although the physiological importance of such apparent autodephosphorylation remains unclear, it appears to be primarily a characteristic of TKDs that closely resemble IRK in terms of the structural details of their autoinhibition and phosphorylation-dependent activation [25, 38, 49].

TrkA TKD autophosphorylates more rapidly than TrkB TKD, with a similar order of phosphorylation site usage that resembles IRK

To analyze Trk TKD autophosphorylation in more detail, we followed the reaction by Western blotting with phospho-specific antibodies – with a view to comparing phosphorylation site usage in addition. Three antibodies were used. One recognizes phosphorylation of the first tyrosine in the pTyrxxxTyr-Tyr motif (pTyr^{676} in TrkA, pTyr^{702} in TrkB). Another recognizes the second and third phosphotyrosines in the TyrxxxpTyr-pTyr motif (pTyr/pTyr$^{680/681}$ in TrkA, pTyr/pTyr$^{706/707}$). The third recognizes the C-terminal tail phosphotyrosine (pTyr^{791} in TrkA, pTyr^{817} in TrkB).

Autophosphorylation studies using 5 μM TKD, at 15°C (Fig. 2), showed a statistically significant difference in phosphorylation of TrkA and TrkB with each of the phosphospecific antibodies at 10 min. In the 2-color Western blots shown in Fig. 2A, the 10 min time-point

shows a clear signal with all three phospho-specific antibodies for TrkA but not TrkB – illustrating a further extension of the lag phase for TrkB autophosphorylation as temperature is reduced. In the plots shown in Fig. 2B, P values for the TrkA/TrkB difference (adjusted using the Bonferroni correction for multiple comparisons) ranged from 0.006 ($pTyr^{791/817}$) to 0.01 ($pTyr^{676/702}$) at 10 min, with no significant differences at other time points. This trend was also maintained at other temperatures (Fig. S4).

The order of autophosphorylation site usage appears to be the same for the TrkA and TrkB TKDs in these experiments, with the activation loop tyrosines being phosphorylated first, and phosphorylation of the C-terminal tail tyrosine (Tyr^{791} in TrkA, Tyr^{817} in TrkB) following (Fig. 2). We used Phos-tag gels [28] to further assess this, as shown in Fig. 3, which show that essentially all of the TKD is phosphorylated within 10 min. We cannot distinguish between TrkA TKD that is singly and triply phosphorylated in the YxxxYY motif using the $pTyr^{676}$ and pTyr/$pTyr^{680/681}$ antibodies. The signals for both of these antibodies increase with the same kinetics, and they recognize bands with the same mobilities in Phos-tag gels – suggesting that the three tyrosines are phosphorylated with very similar kinetics. It is clear from Fig. 3C, however, that Tyr^{791} is phosphorylated later than the YxxxYY motif, as also suggested by Fig. 2B – resulting in the 4p TrkA TKD species in Fig. 3D. TrkB TKD is broadly similar, but the pTyr/$pTyr^{706/707}$ antibody appears to recognize a more mobile (presumed 2p) species at 10 min (Fig. 3B) that is followed at 20 min by a 3p species recognized by the $pTyr^{702}$ antibody (Fig. 3A). Thus, in TrkB TKD, the first Tyr of the YxxxYY motif appears to be phosphorylated after the 706/707 pair. Again, the C-tail tyrosine (Tyr^{817}) is phosphorylated last (Fig. 3C), to yield the 4p species that appears at 30 min (Fig. 3D). With the caveat that we cannot distinguish between species phosphorylated at one or both of the 'YY' tyrosines in the YxxxYY motif, these characteristics appear similar to IRK [50], IGF1-R [37], and MuSK [36]. The TrkA and TrkB TKDs both appears to be phosphorylated first at one of the tyrosines in the YY pair, and then at the first tyrosine of the YxxxYY motif. Tris phosphorylation of this motif occurs late in the reaction for IRK [50], and would not change recognition by the pTyr/$pTyr^{680/681}$ antibody in the case of the Trks. We therefore conclude that phosphorylation site usage of TrkA and TrkB resembles IRK, IGF1-R, and MuSK – with no substantial differences between TrkA and TrkB. Again, the TrkA/B TKDs resemble their closest structural relatives in terms of phosphorylation site usage rather than ALK or c-Met, where the order of YxxxYY phosphorylation appears to be distinct [39, 51–53].

TrkA TKD crystallographic dimer not observed in TrkB TKD crystal structures

Since autophosphorylation of IRK-related tyrosine kinases appears to be intermolecular [37, 50], we hypothesized that the more rapid autophosphorylation seen for the TrkA TKD might reflect a higher preference for self-association than for TrkB TKD. In studies using sedimentation equilibrium analytical ultracentrifugation (SE-AUC) we could see no difference in TKD oligomerization at >10 μM, with both proteins sedimenting as ideal monomers of 34.8 and 35.1 kDa, respectively (Fig. S2). However, in our pilot experiments for kinase assays with dephosphorylated Trk TKDs, we observed a significant concentration dependence in our initial velocity values for TrkA but not TrkB (Fig. S5), and only when the TrkA TKD concentration exceeded approximately 60nM (Fig. S5A). This finding prompted

us to perform the subsequent assays discussed above at concentrations that we established do not influence activity (30 nM for TrkA, 400 nM for TrkB, see Materials and Methods). However, we hypothesized that this phenomenon might be related to the higher autophosphorylation rate seen for TrkA TKD than for TrkB TKD in Figs. 2 and 3, and might reflect a degree of self-association that was not evident in SE-AUC studies. Indeed in our initial crystal structure of the (inactive) TrkA TKD – PDB ID 4GT5 [25] we observed two crystallographic dimers (Fig. 4A,B) that searches using the PISA server [54] identified in 23 additional TrkA TKD crystal structures that have since been deposited to the Protein Data Bank (PDB). It should be noted that there are an additional 24 PDB entries for TrkA TKD that show different crystal packing – so the TrkA TKD does not always crystallize in the dimers shown in Fig. 4A and B. However, the 24 cases in which it is seen represent at least 3 different crystal forms/environments and bury a total surface area of 1,290 $Å^2$ (Fig. 4A) or 1,250 $Å^2$ in PDB ID 4GT5 (Fig. 4B). Similar packing is not seen in the 4 TrkB TKD structure entries in the PDB. Importantly, the two TrkA TKD dimers involve residues that differ between TrkA and TrkB (Fig. 4C). For the 'face-to-face' dimer in Fig. 4A, side chains of residues between αEF and αF and in αG that differ between TrkA and TrkB contribute to the dimer, notably the side-chains of Thr^{734} (Asn in TrkB), Asp^{738} (Glu in TrkB) and Leu^{700} (Met in TrkB), marked in both Fig, 4A and (with arrows) in Fig. 4C. The other dimer is largely mediated by the kinase insert domain (KID), which is the region of greatest sequence divergence between TrkA and TrkB (which are 76% identical) as shown in Fig. 4C.

Stabilization of the face-to-face dimer for TrkA as a result of the sequence differences between the two TKDs in its interface could promote its *trans*-autophosphorylation compared with that of TrkB, and this might explain our findings. It seems more plausible, however, that the KID-mediated dimer is the key. TrkA-specific residues play a key role in interactions between the two TKDs in this dimer, with Glu^{615} playing a key role, interacting across the interface with Arg^{593} in the hinge region of the dimer partner (Fig. 5). Asp^{616} in the KID also plays a key role in setting up this interaction, forming predicted hydrogen bonds with Arg^{593} and His^{594} in its own hinge region. The fact that KID residues that seem to mediate the TrkA TKD 'KID' dimer shown in Fig. 4B also interact with residues in the hinge region of the kinase domain further suggests that dimerization might modulate conformational dynamics in the hinge region to alter TKD activity – as has been reported for other kinases [55, 56]. Moreover, as pointed out by Bertrand *et al.* [57], there are no such interactions in TrkB, and no similar dimer has been seen in TrkB TKD crystals.

KID mutations in TrkA mutant slow progression of TKD autophosphorylation

The results outlined above prompted us to hypothesize that swapping the TrkA KID for the TrkB KID would yield a TKD that resembles TrkB in autophosphorylation assays. We therefore mutated the TrkA KID to resemble that seen in TrkB as shown in Fig. 5A, to yield $TrkA^{B\text{-}KID}$. The $TrkA^{B\text{-}KID}$ TKD has a shorter KID (by 2 residues) and lacks Glu^{615} and Asp^{616}, which are central in intermolecular and intramolecular interactions respectively in the TrkA TKD KID/hinge dimer as mentioned above (see Fig, 5B). To examine the functional consequences of this change we used a radioactive autophosphorylation assay to compare autophosphorylation profiles for TrkA, $TrkA^{B\text{-}KID}$, and TrkB TKDs. As shown in Fig. 5C, TrkA (at 4 μM) became autophosphorylated significantly more rapidly than TrkB

TKD as expected, with significant differences at 1.5, 2, 3, and 4 min (after which TrkB catches up). The $TrkA^{B\text{-}KID}$ variant showed a slightly slower rate of autophosphorylation than wild-type TrkA TKD, but was not reduced to the rate seen for TrkB TKD. Unpaired Student's *t*-tests suggested significant differences ($P < 0.05$) at the 2, 3, and 4 min time points (Fig. 5C), although significance was lost following correction for multiple comparisons using the Bonferroni method. Taken together, these data are consistent with the crystallographically observed TrkA TKD dimer interface shown in Fig. 4B playing some role in the accelerated autophosphorylation of TrkA TKD. However, the effect is clearly only partial, possibly because we did not fully abolish dimerization with the KID mutations made, and possibly because both dimers seen across multiple TrkA TKD crystal structures play a role.

Knockdown of p75 converts TrkB (but not TrkA) signaling from sustained to transient

As mentioned in the Introduction, the initial motivation for this project was to understand why upregulated TrkB signaling causes cell proliferation and a poor prognosis in neuroblastoma, whereas TrkA conversely promotes cell differentiation and a favorable prognosis [2, 3, 5, 6]. The TrkA TKD autophosphorylates more rapidly than TrkB TKD *in vitro*, which might suggest a difference in signaling kinetics for these two neurotrophin receptors. Moreover, subtle differences in signaling outcome have been reported when optogenetic activation of the membrane-associated intracellular regions of TrkA and TrkB was compared in Xenopus embryos [21]. It is well established, with TrkA as a key subject of the early studies in PC12 cells, that signaling kinetics can define cellular outcome. Sustained ERK signaling correlates with cell differentiation and transient ERK activation with cell proliferation [8, 9]. NGF stimulates neurite outgrowth in parental PC12 cells, and BDNF also stimulates neurite outgrowth in PC12 cells engineered to express TrkB [58] – which they do not normally express [59]. As shown in Fig. 6A, this is associated with sustained activation of TrkB and ERK by BDNF. A similar signaling profile can also be recapitulated by sustained optogenetically-induced TrkB dimerization [60]. However, there have been several reports that TrkB signaling kinetics can be altered, in particular by neuronal activity [24, 61], to make it more transient. We also recently showed for the EGF receptor that the same RTK can signal either in a transient manner (leading to proliferation) or a sustained manner (to promote differentiation), depending on how it is activated [14, 15]. Such a difference – dependent on cellular context – may explain why TrkB promotes proliferation in neuroblastoma, but differentiation in PC12 cells.

One other aspect of neurotrophin signaling that correlates with an improved prognosis in neuroblastoma is expression of the low affinity p75 neurotrophin receptor, $p75^{NTR}$ [23]. $p75^{NTR}$ is well known to promote NGF-induced TrkA signaling and support differentiation of sympathetic neurons [62], and also facilitates the ability of TrkB to promote neuronal survival [63]. Upregulation of $p75^{NTR}$ appears to reduce the tumorigenicity of neuroblastoma cells *in vivo* [22]. Since $p75^{NTR}$ interacts with TrkB and facilitates its ability to promote neuronal survival [63], we wondered if knocking down $p75^{NTR}$ in TrkB-PC12 cells would make BDNF-induced TrkB signaling more transient. As shown in Fig. 6B,C, depleting $p75^{NTR}$ from TrkB-PC12 cells by siRNA made BDNF-induced TrkB activation more transient, consistent with the association of higher $p75^{NTR}$ levels with better tumor

phenotypes. By contrast, Negrini *et al.* previously reported that TrkA responses to NGF remain sustained in parental PC12 cells lacking $p75^{NTR}$ [64], which we confirmed (Fig. 6D). We therefore suggest that interaction with $p75^{NTR}$ has different effects on the kinetics of ligand-induced signaling by TrkA and TrkB, and may be required for TrkB (but not TrkA) signaling to be fully sustained. We speculate that this difference could be related to the ability of the TrkA TKD to self-associate and *trans*-autophosphorylate more efficiently than TrkB TKD without facilitation of dimerization by $p75^{NTR}$.

CONCLUSIONS

The TrkA and TrkB neurotrophin receptors are homologous RTKs that initiate broadly similar signaling pathways upon ligand-induced activation of their TKDs [65]. However, several reports have demonstrated that TrkA and TrkB expression and activation can result in distinct cellular outcomes in the same cell type [4, 7, 58, 66]. This is particularly notable in neuroblastoma, where TrkB signaling correlates with a poor prognosis, and TrkA signaling with a favorable one [2, 67]. Our biochemical analysis of the TrkA and TrkB TKDs uncovered no substantial differences that can satisfyingly explain the distinct signaling of the two receptors on their own, but did find that TrkA TKD autophosphorylates faster than TrkB TKD *in vitro*. The initial lag phase seen for TrkB, and its slower autophosphorylation, might allow protein tyrosine phosphatases to ‘compete’ more effectively with kinase activity to make TrkB activation more transient than that of TrkA. NGF-induced TrkA signaling has been well studied, and its sustained nature has underpinned studies that link signaling kinetics to cellular outcome – with sustained responses promoting differentiation and transient responses promoting proliferation. If TrkB signaling is intrinsically more transient, this could explain its association with proliferation and poor prognosis in neuroblastoma, and the contrast with TrkA’s association with favorable outcome.

Interestingly the differences between TrkA and TrkB, which seem to depend in part on deviations in sequence of the kinase insert domain, resemble distinctions reported between the non-receptor tyrosine kinases Itk and Btk [68]. By making Itk/Btk chimeras, Joseph *et al.* reported that an increase in Itk’s catalytic efficiency ($k_{cat}/K_{m,\ ATP}$) of just ~3.5-fold was sufficient to make its signaling more Btk-like, with enhanced, more prolonged signaling of the receptor that controls it [68]. This also correlated with enhanced activation loop phosphorylation. These findings resemble the situation with TrkA, which has a ~2-fold higher catalytic efficiency than TrkB (Table 1), and is more readily phosphorylated – possibly to allow a more readily activatable and sustained response. Along similar lines, studies of autophosphorylation kinetics of the fibroblast growth factor receptor (FGFR)-1 and −2 [69] have shown that FGFR2’s TKD is less stringently autoinhibited than that of FGFR1, leading to faster in vitro autophosphorylation kinetics for FGFR2. This may explain some signaling differences between these receptors, where signaling duration determines phenotype [16, 17, 70] – as we are suggesting for TrkA and TrkB. The differences might arise through kinetic proofreading-type effects [71] or through differences in trafficking that have been described for TrkA and TrkB [72, 73], and might control access to intracellular tyrosine phosphatases as described for EGFR [74].

Several recent studies have indicated that the phenotypic outcome of cell signaling by RTKs depends on the kinetics of receptor activation itself [12–15]. The studies described here for TrkA and TrkB suggest that even subtle differences can be important – consistent with previous results for FGFR isoforms as well as Itk and Btk [16, 17, 68, 75]. The link between poor prognosis in neuroblastoma and TrkB signaling may reflect its more stringent autoinhibition and ability to signal transiently in certain cellular contexts such as those in neuroblastoma, whereas TrkA signaling remains sustained – promoting differentiation and more favorable outcome. With selective inhibition of one Trk isoform over another remaining a major therapeutic challenge [76], these data suggest that exploiting differential kinetics at intermediate inhibitor doses may have some value in certain settings.

Supplementary Material

Refer to Web version on PubMed Central for supplementary material.

ACKNOWLEDGEMENTS

We thank Kate Ferguson and members of the Lemmon and Ferguson labs for advice and reading of the manuscript, and Dr. Garrett Brodeur for providing TrkA and TrkB cDNAs. This work was funded in part by NIH grants R01-GM099891 and R35-GM122485 (to M.A.L.) and training grant funds to S.C.A. (T32-GM008275).

Abbreviations used:

ALK	anaplastic lymphoma kinase
BDNF	brain-derived neurotrophic factor
CT	c-terminal tail
C-lobe	C-terminal lobe
DTT	dithiothreitol
EGFR	epidermal growth factor receptor
ERK	extracellular signal-regulated kinase
FGFR	fibroblast growth factor receptor
IGF1R	insulin-like growth factor-1 receptor
IRK	insulin receptor kinase
JM	juxtamembrane
KID	kinase insert domain
MuSK	muscle-specific kinase
NCBI	National Center for Biotechnology Information
NGF	nerve growth factor

Ni-NTA	Ni^{2+}-nitrilotriacetate
N-lobe	amino-terminal lobe
PDB	protein data bank
RT	room temperature
RTK	receptor tyrosine kinase
TKD	tyrosine kinase domain
Trk	tropomyosin-reeceptor kinase

REFERENCES

1. Martin-Zanca D, Hughes SH and Barbacid M (1986) A human oncogene formed by the fusion of truncated tropomyosin and protein tyrosine kinase sequences. Nature 319, 743–748 10.1038/319743a0 [PubMed: 2869410]
2. Schramm A, Schulte JH, Astrahantseff K, Apostolov O, van Limpt V, Sieverts H, Kuhfittig-Kulle S, Pfeiffer P, Versteeg R and Eggert A (2005) Biological effects of TrkA and TrkB receptor signaling in neuroblastoma. Cancer Lett. 228, 143–153 10.1016/j.canlet.2005.02.051 [PubMed: 15921851]
3. Brodeur GM, Minturn JE, Ho R, Simpson AM, Iyer R, Varela CR, Light JE, Kolla V and Evans AE (2009) Trk receptor expression and inhibition in neuroblastomas. Clin. Cancer Res 15, 3244–3250 10.1158/1078-0432.CCR-08-1815 [PubMed: 19417027]
4. Lucarelli E, Kaplan D and Thiele CJ (1997) Activation of trk-A but not trk-B signal transduction pathway inhibits growth of neuroblastoma cells. Eur. J. Cancer 33, 2068–2070 10.1016/s0959-8049(97)00266-9 [PubMed: 9516854]
5. Nakagawara A, Arima-Nakagawara M, Scavarda NJ, Azar CG, Cantor AB and Brodeur GM (1993) Association between high levels of expression of the TRK gene and favorable outcome in human neuroblastoma. N. Engl. J. Med 328, 847–854 10.1056/NEJM199303253281205 [PubMed: 8441429]
6. Nakagawara A, Azar CG, Scavarda NJ and Brodeur GM (1994) Expression and function of TRK-B and BDNF in human neuroblastomas. Mol. Cell. Biol 14, 759–767 10.1128/mcb.14.1.759 [PubMed: 8264643]
7. Schulte JH, Schramm A, Klein-Hitpass L, Klenk M, Wessels H, Hauffa BP, Eils J, Eils R, Brodeur GM, Schweigerer L, Havers W and Eggert A (2005) Microarray analysis reveals differential gene expression patterns and regulation of single target genes contributing to the opposing phenotype of TrkA- and TrkB-expressing neuroblastomas. Oncogene 24, 165–177 10.1038/sj.onc.1208000 [PubMed: 15637590]
8. Murphy LO and Blenis J (2006) MAPK signal specificity: the right place at the right time. Trends Biochem. Sci 31, 268–275 10.1016/j.tibs.2006.03.009 [PubMed: 16603362]
9. Marshall CJ (1995) Specificity of receptor tyrosine kinase signaling: transient versus sustained extracellular signal-regulated kinase activation. Cell 80, 179–185 10.1016/0092-8674(95)90401-8 [PubMed: 7834738]
10. Murphy LO, MacKeigan JP and Blenis J (2004) A network of immediate early gene products propagates subtle differences in mitogen-activated protein kinase signal amplitude and duration. Mol. Cell. Biol 24, 144–153 10.1128/mcb.24.1.144-153.2004 [PubMed: 14673150]
11. Bugaj LJ, Sabnis AJ, Mitchell A, Garbarino JE, Toettcher JE, Bivona TG and Lim WA (2018) Cancer mutations and targeted drugs can disrupt dynamic signal encoding by the Ras-Erk pathway. Science 361, eaao3048 10.1126/science.aao3048 [PubMed: 30166458]
12. Toettcher JE, Weiner OD and Lim WA (2013) Using optogenetics to interrogate the dynamic control of signal transmission by the Ras/Erk module. Cell 155, 1422–1434 10.1016/j.cell.2013.11.004 [PubMed: 24315106]

13. Sparta B, Pargett M, Minguet M, Distor K, Bell G and Albeck JG (2015) Receptor level mechanisms are required for epidermal growth factor (EGF)-stimulated extracellular signal-regulated kinase (ERK) activity pulses. J. Biol. Chem 290, 24784–24792 10.1074/jbc.M115.662247 [PubMed: 26304118]
14. Kiyatkin A, van Alderwerelt van Rosenburgh IK, Klein DE and Lemmon MA (2020) Kinetics of receptor tyrosine kinase activation define ERK signaling dynamics. Sci. Signal 13, eaaz5267 10.1126/scisignal.aaz5267 [PubMed: 32817373]
15. Freed DM, Bessman NJ, Kiyatkin A, Salazar-Cavazos E, Byrne PO, Moore JO, Valley CC, Ferguson KM, Leahy DJ, Lidke DS and Lemmon MA (2017) EGFR ligands differentially stabilize receptor dimers to specify signaling kinetics. Cell 171, 683–695 10.1016/j.cell.2017.09.017 [PubMed: 28988771]
16. Huang Z, Tan Y, Gu J, Liu Y, Song L, Niu J, Zhao L, Srinivasan L, Lin Q, Deng J, Li Y, Conklin DJ, Neubert TA, Cai L, Li X and Mohammadi M (2017) Uncoupling the mitogenic and metabolic functions of FGF1 by tuning FGF1-FGF receptor dimer stability. Cell Rep. 20, 1717–1728 10.1016/j.celrep.2017.06.063 [PubMed: 28813681]
17. Ahmed Z, Schüller AC, Suhling K, Tregidgo C and Ladbury JE (2008) Extracellular point mutations in FGFR2 elicit unexpected changes in intracellular signalling. Biochem. J 413, 37–49 10.1042/BJ20071594 [PubMed: 18373495]
18. Ho CCM, Chhabra A, Starkl P, Schnorr PJ, Wilmes S, Moraga I, Kwon HS, Gaudenzio N, Sibilano R, Wehrman TS, Gakovic M, Sockolosky JT, Tiffany MR, Ring AM, Piehler J, Weissman IL, Galli SJ, Shizuru JA and Garcia KC (2017) Decoupling the functional pleiotropy of stem cell factor by tuning c-Kit signaling. Cell 168, 1041–1052 10.1016/j.cell.2017.02.011 [PubMed: 28283060]
19. Muragaki Y, Chou TT, Kaplan DR, Trojanowski JQ and Lee VM (1997) Nerve growth factor induces apoptosis in human medulloblastoma cell lines that express TrkA receptors. J. Neurosci 17, 530–542 10.1523/JNEUROSCI.17-02-00530.1997 [PubMed: 8987776]
20. McGregor LM, McCune BK, Graff JR, McDowell PR, Romans KE, Yancopoulos GD, Ball DW, Baylin SB and Nelkin BD (1999) Roles of trk family neurotrophin receptors in medullary thyroid carcinoma development and progression. Proc. Natl. Acad. Sci. U.S.A 96, 4540–4545 10.1073/pnas.96.8.4540 [PubMed: 10200298]
21. Krishnamurthy VV, Fu J, Oh TJ, Khamo J, Yang J and Zhang K (2020) A generalizable optogenetic strategy to regulate receptor tyrosine kinases during vertebrate embryonic development. J. Mol. Biol 432, 3149–3158 10.1016/j.jmb.2020.03.032 [PubMed: 32277988]
22. Schulte JH, Pentek F, Hartmann W, Schramm A, Friedrichs N, Øra I, Koster J, Versteeg R, Kirfel J, Buettner R and Eggert A (2009) The low-affinity neurotrophin receptor, p75, is upregulated in ganglioneuroblastoma/ganglioneuroma and reduces tumorigenicity of neuroblastoma cells in vivo. Int. J. Cancer 124, 2488–2494 10.1002/ijc.24204 [PubMed: 19142969]
23. Ho R, Minturn JE, Simpson AM, Iyer R, Light JE, Evans AE and Brodeur GM (2011) The effect of P75 on Trk receptors in neuroblastomas. Cancer Lett. 305, 76–85 10.1016/j.canlet.2011.02.029 [PubMed: 21419569]
24. Guo W, Nagappan G and Lu B (2018) Differential effects of transient and sustained activation of BDNF-TrkB signaling. Dev. Neurobiol 78, 647–659 10.1002/dneu.22592 [PubMed: 29575722]
25. Artim SC, Mendrola JM and Lemmon MA (2012) Assessing the range of kinase autoinhibition mechanisms in the insulin receptor family. Biochem. J 448, 213–220 10.1042/BJ20121365 [PubMed: 22992069]
26. Zhuo S, Clemens JC, Hakes DJ, Barford D and Dixon JE (1993) Expression, purification, crystallization, and biochemical characterization of a recombinant protein phosphatase. J. Biol. Chem 268, 17754–17761 [PubMed: 8394350]
27. Bresler SC, Wood AC, Haglund EA, Courtright J, Belcastro LT, Plegaria JS, Cole K, Toporovskaya Y, Zhao H, Carpenter EL, Christensen JG, Maris JM, Lemmon MA and Mossé YP (2011) Differential inhibitor sensitivity of anaplastic lymphoma kinase variants found in neuroblastoma. Sci. Transl. Med 3, 108ra114 10.1126/scitranslmed.3002950
28. Kinoshita E and Kinoshita-Kikuta E (2011) Improved Phos-tag SDS-PAGE under neutral pH conditions for advanced protein phosphorylation profiling. Proteomics 11, 319–323 10.1038/nprot.2009.154 [PubMed: 21204258]

29. Segal RA, Bhattacharyya A, Rua LA, Alberta JA, Stephens RM, Kaplan DR and Stiles CD (1996) Differential utilization of Trk autophosphorylation sites. J. Biol. Chem 271, 20175–20181 10.1074/jbc.271.33.20175 [PubMed: 8702742]
30. Choi DY, Toledo-Aral JJ, Segal R and Halegoua S (2001) Sustained signaling by phospholipase C-gamma mediates nerve growth factor-triggered gene expression. Mol. Cell. Biol 21, 2695–2705 10.1128/MCB.21.8.2695-2705.2001 [PubMed: 11283249]
31. Guiton M, Gunn-Moore FJ, Stitt TN, Yancopoulos GD and Tavaré JM (1994) Identification of in vivo brain-derived neurotrophic factor-stimulated autophosphorylation sites on the TrkB receptor tyrosine kinase by site-directed mutagenesis. J. Biol. Chem 269, 30370–30377 [PubMed: 7982951]
32. Middlemas DS, Meisenhelder J and Hunter T (1994) Identification of TrkB autophosphorylation sites and evidence that phospholipase C-gamma 1 is a substrate of the TrkB receptor. J. Biol. Chem 269, 5458–5466 [PubMed: 8106527]
33. Stephens RM, Loeb DM, Copeland TD, Pawson T, Greene LA and Kaplan DR (1994) Trk receptors use redundant signal transduction pathways involving SHC and PLC-gamma 1 to mediate NGF responses. Neuron 12, 691–705 10.1016/0896-6273(94)90223-2 [PubMed: 8155326]
34. Li S, Covino ND, Stein EG, Till JH and Hubbard SR (2003) Structural and biochemical evidence for an autoinhibitory role for tyrosine 984 in the juxtamembrane region of the insulin receptor. J. Biol. Chem 278, 26007–26014 10.1074/jbc.M302425200 [PubMed: 12707268]
35. Li W and Miller WT (2006) Role of the activation loop tyrosines in regulation of the insulin-like growth factor I receptor-tyrosine kinase. J. Biol. Chem 281, 23785–23791 10.1074/jbc.M605269200 [PubMed: 16793764]
36. Till JH, Becerra M, Watty A, Lu Y, Ma Y, Neubert TA, Burden SJ and Hubbard SR (2002) Crystal structure of the MuSK tyrosine kinase: insights into receptor autoregulation. Structure 10, 1187–1196 10.1016/s0969-2126(02)00814-6 [PubMed: 12220490]
37. Favelyukis S, Till JH, Hubbard SR and Miller WT (2001) Structure and autoregulation of the insulin-like growth factor 1 receptor kinase. Nature Struct. Bio 8, 1058–1063 10.1038/nsb721 [PubMed: 11694888]
38. Hubbard SR, Wei L, Ellis L and Hendrickson WA (1994) Crystal structure of the tyrosine kinase domain of the human insulin receptor. Nature 372, 746–754 10.1038/372746a0 [PubMed: 7997262]
39. Timofeevski SL, McTigue MA, Ryan K, Cui J, Zou HY, Zhu JX, Chau F, Alton G, Karlicek S, Christensen JG and Murray BW (2009) Enzymatic characterization of c-Met receptor tyrosine kinase oncogenic mutants and kinetic studies with aminopyridine and triazolopyrazine inhibitors. Biochemistry 48, 5339–5349 10.1021/bi900438w [PubMed: 19459657]
40. Schlessinger J (1979) Receptor aggregation as a mechanism for transmembrane signaling: Models for hormone action In Physical Chemistry of Cell Surface Events in Cellular Regulation (De Lisi C a. B. R, ed.). pp. 89–118, Elsevier
41. Lemmon MA, Bu Z, Ladbury JE, Zhou M, Pinchasi D, Lax I, Engelman DM and Schlessinger J (1997) Two EGF molecules contribute additively to stabilization of the EGFR dimer. EMBO J. 16, 281–294 10.1093/emboj/16.2.281 [PubMed: 9029149]
42. Iwasaki Y, Nishiyama H, Suzuki K and Koizumi S (1997) Sequential cis/trans autophosphorylation in TrkB tyrosine kinase. Biochemistry 36, 2694–2700 10.1021/bi962057x [PubMed: 9054577]
43. Gruppuso PA, Boylan JM, Levine BA and Ellis L (1992) Insulin receptor tyrosine kinase domain auto-dephosphorylation. Biochem. Biophys. Res. Commun 189, 1457–1463 10.1016/0006-291x(92)90238-g [PubMed: 1336369]
44. Argetsinger LS and Shafer JA (1992) The reversible and irreversible autophosphorylations of insulin receptor kinase. J. Biol. Chem 267, 22095–22101 [PubMed: 1385393]
45. Pike LJ, Eakes AT and Krebs EG (1986) Characterization of affinity-purified insulin receptor/kinase. Effects of dithiothreitol on receptor/kinase function. J. Biol. Chem 261, 3782–3789 [PubMed: 3005300]

46. al-Hasani H, Passlack W and Klein HW (1994) Phosphoryl exchange is involved in the mechanism of the insulin receptor kinase. FEBS Letts. 349, 17–22 10.1016/0014-5793(94)00632-6 [PubMed: 8045295]
47. Bae JH, Boggon TJ, Tomé F, Mandiyan V, Lax I and Schlessinger J (2010) Asymmetric receptor contact is required for tyrosine autophosphorylation of fibroblast growth factor receptor in living cells. Proc. Natl. Acad. Sci. U.S.A 107, 2866–2871 10.1073/pnas.0914157107 [PubMed: 20133753]
48. Parast CV, Mroczkowski B, Pinko C, Misialek S, Khambatta G and Appelt K (1998) Characterization and kinetic mechanism of catalytic domain of human vascular endothelial growth factor receptor-2 tyrosine kinase (VEGFR2 TK), a key enzyme in angiogenesis. Biochemistry 37, 16788–16801 10.1021/bi981291f [PubMed: 9843450]
49. Hubbard SR (2013) The insulin receptor: both a prototypical and atypical receptor tyrosine kinase. Cold Spring Harb. Perspect. Biol 5, a008946 10.1101/cshperspect.a008946 [PubMed: 23457259]
50. Wei L, Hubbard SR, Hendrickson WA and Ellis L (1995) Expression, characterization, and crystallization of the catalytic core of the human insulin receptor protein-tyrosine kinase domain. J. Biol. Chem 270, 8122–8130 10.1074/jbc.270.14.8122 [PubMed: 7713916]
51. Longati P, Bardelli A, Ponzetto C, Naldini L and Comoglio PM (1994) Tyrosines 1234–1235 are critical for activation of the tyrosine kinase encoded by the MET proto-oncogene (HGF receptor). Oncogene 9, 49–57 [PubMed: 8302603]
52. Tartari CJ, Gunby RH, Coluccia AM, Sottocornola R, Cimbro B, Scapozza L, Donella-Deana A, Pinna LA and Gambacorti-Passerini C (2008) Characterization of some molecular mechanisms governing autoactivation of the catalytic domain of the anaplastic lymphoma kinase. J. Biol. Chem 283, 3743–3750 10.1074/jbc.M706067200 [PubMed: 18070884]
53. Chiara F, Michieli P, Pugliese L and Comoglio PM (2003) Mutations in the met oncogene unveil a “dual switch” mechanism controlling tyrosine kinase activity. J. Biol. Chem 278, 29352–29358 10.1074/jbc.M302404200 [PubMed: 12746450]
54. Krissinel E and Henrick K (2007) Inference of macromolecular assemblies from crystalline state. J. Mol. Biol 372, 774–797 10.1016/j.jmb.2007.05.022 [PubMed: 17681537]
55. Sours KM, Xiao Y and Ahn NG (2014) Extracellular-regulated kinase 2 is activated by the enhancement of hinge flexibility. J. Mol. Biol 426, 1925–1935 10.1016/j.jmb.2014.02.011 [PubMed: 24534729]
56. Chen H, Ma J, Li W, Eliseenkova AV, Xu C, Neubert TA, Miller WT and Mohammadi M (2007) A molecular brake in the kinase hinge region regulates the activity of receptor tyrosine kinases. Mol. Cell 27, 717–730 10.1016/j.molcel.2007.06.028 [PubMed: 17803937]
57. Bertrand T, Kothe M, Liu J, Dupuy A, Rak A, Berne PF, Davis S, Gladysheva T, Valtre C, Crenne JY and Mathieu M (2012) The crystal structures of TrkA and TrkB suggest key regions for achieving selective inhibition. J. Mol. Biol 423, 439–453 10.1016/j.jmb.2012.08.002 [PubMed: 22902478]
58. Iwasaki Y, Ishikawa M, Okada N and Koizumi S (1997) Induction of a distinct morphology and signal transduction in TrkB/PC12 cells by nerve growth factor and brain-derived neurotrophic factor. J. Neurochem 68, 927–934 10.1046/j.1471-4159.1997.68030927.x [PubMed: 9048737]
59. Kaplan DR, Martin-Zanca D and Parada LF (1991) Tyrosine phosphorylation and tyrosine kinase activity of the trk proto-oncogene product induced by NGF. Nature 350, 158–160 10.1038/350158a0 [PubMed: 1706478]
60. Chang K-Y, Woo D, Jung H, Lee S, Kim S, Won J, Kyung T, Park H, Kim N, Yang HW, Park J-Y, Hwang EM, Kim D and Heo WD (2014) Light-inducible receptor tyrosine kinases that regulate neurotrophin signalling. Nat. Commun 5, 4057 10.1038/ncomms5057 [PubMed: 24894073]
61. Guo W, Ji Y, Wang S, Sun Y and Lu B (2014) Neuronal activity alters BDNF-TrkB signaling kinetics and downstream functions. J. Cell Sci 127, 2249–2260 10.1242/jcs.139964 [PubMed: 24634513]
62. Hempstead BL, Martin-Zanca D, Kaplan DR, Parada LF and Chao MV (1991) High-affinity NGF binding requires coexpression of the trk proto-oncogene and the low-affinity NGF receptor. Nature 350, 678–683 10.1038/350678a0 [PubMed: 1850821]

63. Zanin JP, Montroull LE, Volosin M and Friedman WJ (2019) The p75 neurotrophin receptor facilitates TrkB signaling and function in rat hippocampal neurons. Front Cell. Neurosci 13, 485 10.3389/fncel.2019.00485 [PubMed: 31736712]
64. Negrini S, D'Alessandro R and Meldolesi J (2013) NGF signaling in PC12 cells: the cooperation of p75(NTR) with TrkA is needed for the activation of both mTORC2 and the PI3K signalling cascade. Biol. Open 2, 855–866 10.1242/bio.20135116 [PubMed: 23951412]
65. Deinhardt K and Chao MV (2014) Trk receptors. Handb. Exp. Pharmacol 220, 103–119 10.1007/978-3-642-45106-5_5 [PubMed: 24668471]
66. Kim CJ, Matsuo T, Lee KH and Thiele CJ (1999) Up-regulation of insulin-like growth factor-II expression is a feature of TrkA but not TrkB activation in SH-SY5Y neuroblastoma cells. Am. J. Pathol 155, 1661–1670 10.1016/S0002-9440(10)65481-8 [PubMed: 10550322]
67. Thiele CJ, Li Z and McKee AE (2009) On Trk--the TrkB signal transduction pathway is an increasingly important target in cancer biology. Clin. Cancer Res 15, 5962–5967 10.1158/1078-0432.CCR-08-0651 [PubMed: 19755385]
68. Joseph RE, Kleino I, Wales TE, Xie Q, Fulton DB, Engen JR, Berg LJ and Andreotti AH (2013) Activation loop dynamics determine the different catalytic efficiencies of B cell- and T cell-specific tec kinases. Sci. Signal 6, ra76 10.1126/scisignal.2004298 [PubMed: 23982207]
69. Lew ED, Bae JH, Rohmann E, Wollnik B and Schlessinger J (2007) Structural basis for reduced FGFR2 activity in LADD syndrome: Implications for FGFR autoinhibition and activation. Proc. Natl. Acad. Sci. U.S.A 104, 19802–19807 10.1073/pnas.0709905104 [PubMed: 18056630]
70. Xian W, Schwertfeger KL and Rosen JM (2007) Distinct roles of fibroblast growth factor receptor 1 and 2 in regulating cell survival and epithelial-mesenchymal transition. Mol. Endocrinol 21, 987–1000 10.1210/me.2006-0518 [PubMed: 17284663]
71. Lemmon MA, Freed DM, Schlessinger J and Kiyatkin A (2016) The dark side of cell signaling: Positive roles for negative regulators. Cell 164, 1172–1184 10.1016/j.cell.2016.02.047 [PubMed: 26967284]
72. Chen ZY, Ieraci A, Tanowitz M and Lee FS (2005) A novel endocytic recycling signal distinguishes biological responses of Trk neurotrophin receptors. Mol. Biol. Cell 16, 5761–5772 10.1091/mbc.e05-07-0651 [PubMed: 16207814]
73. Barford K, Deppmann C and Winckler B (2017) The neurotrophin receptor signaling endosome: Where trafficking meets signaling. Dev. Neurobiol 77, 405–418 10.1002/dneu.22427 [PubMed: 27503831]
74. Stanoev A, Mhamane A, Schuermann KC, Grecco HE, Stallaert W, Baumdick M, Brüggemann Y, Joshi MS, Roda-Navarro P, Fengler S, Stockert R, Roßmannek L, Luig J, Koseska A and Bastiaens PIH (2018) Interdependence between EGFR and phosphatases spatially established by vesicular dynamics generates a growth factor sensing and responding network. Cell Syst. 7, 295–309 10.1016/j.cels.2018.06.006 [PubMed: 30145116]
75. Schüller AC, Ahmed Z and Ladbury JE (2008) Extracellular point mutations in FGFR2 result in elevated ERK1/2 activation and perturbation of neuronal differentiation. Biochem. J 410, 205–211 10.1042/BJ20070859 [PubMed: 18039182]
76. Drilon A (2019) TRK inhibitors in TRK fusion-positive cancers. Ann. Oncol 30 Suppl 8, viii23–viii30 10.1093/annonc/mdz282
77. Louis-Jeune C, Andrade-Navarro MA and Perez-Iratxeta C (2011) Prediction of protein secondary structure from circular dichroism using theoretically derived spectra. Proteins 80, 374–381 10.1002/prot.23188 [PubMed: 22095872]

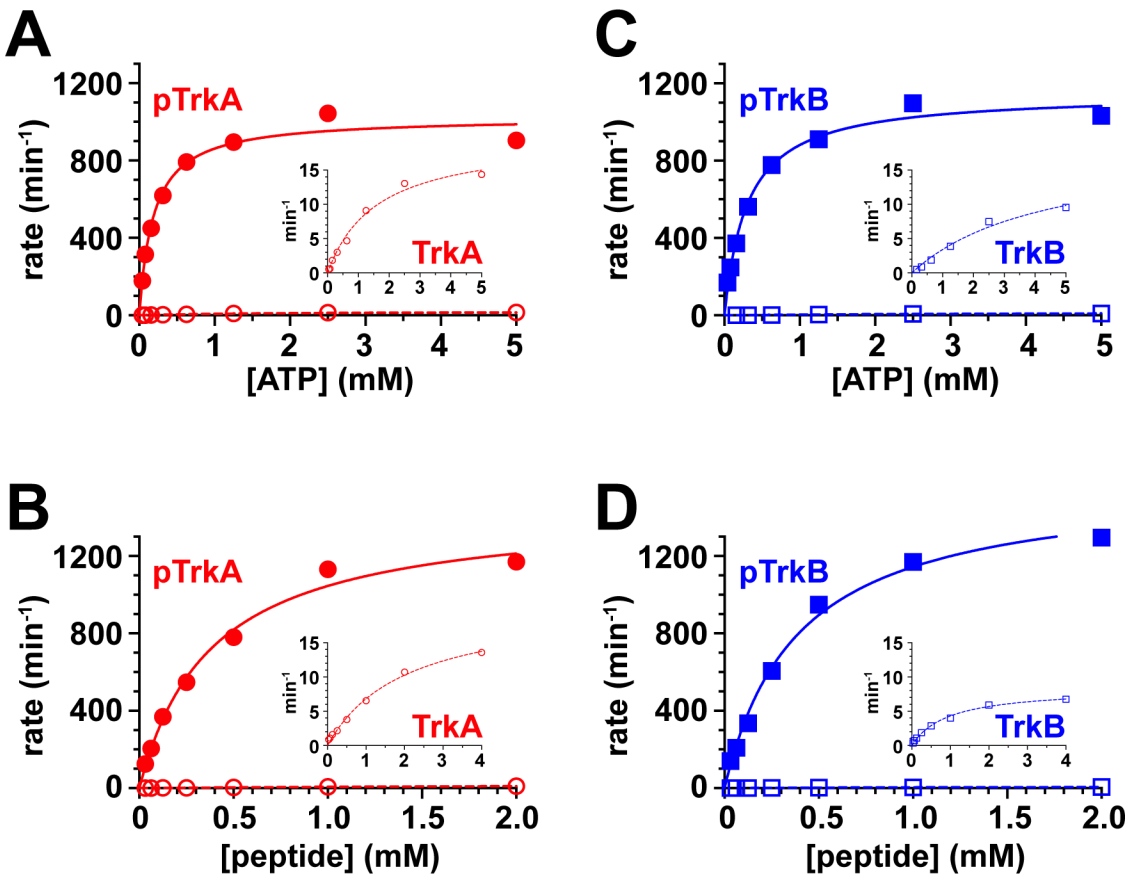

FIGURE 1: Representative kinetic data for TrkA and TrkB TKDs

Representative Michaelis-Menten plots for determining k_{cat} for TrkA (**A,B**) and TrkB (**C,D**) as well as $K_{m,\ ATP}$ (**A,C**) and $K_{m,\ peptide}$ (**B,D**) for the two TKDs. For $K_{m,\ ATP}$ determinations, TKDs were assayed at a range of ATP concentrations (0.039 mM to 5 mM) in the presence of a fixed 2 mM peptide substrate and 10 mM $MgCl_2$. For $K_{m,\ peptide}$ determinations, TKDs were assayed at a range of peptide concentrations (0.031 mM to 4 mM) with fixed (2 mM) ATP and 10 mM $MgCl_2$. Enzyme concentrations were 8 nM for phosphorylated TKDs, 30 nM for dephosphorylated TrkA TKD (**A,B** inserts) or 400 nM for dephosphorylated TrkB TKD (**C,D** inserts). Rates are quoted in units of min^{-1}, normalized per mole of enzyme. Experiments were repeated at least three times, and mean values ± S.D. for each parameter are listed in Table 1.

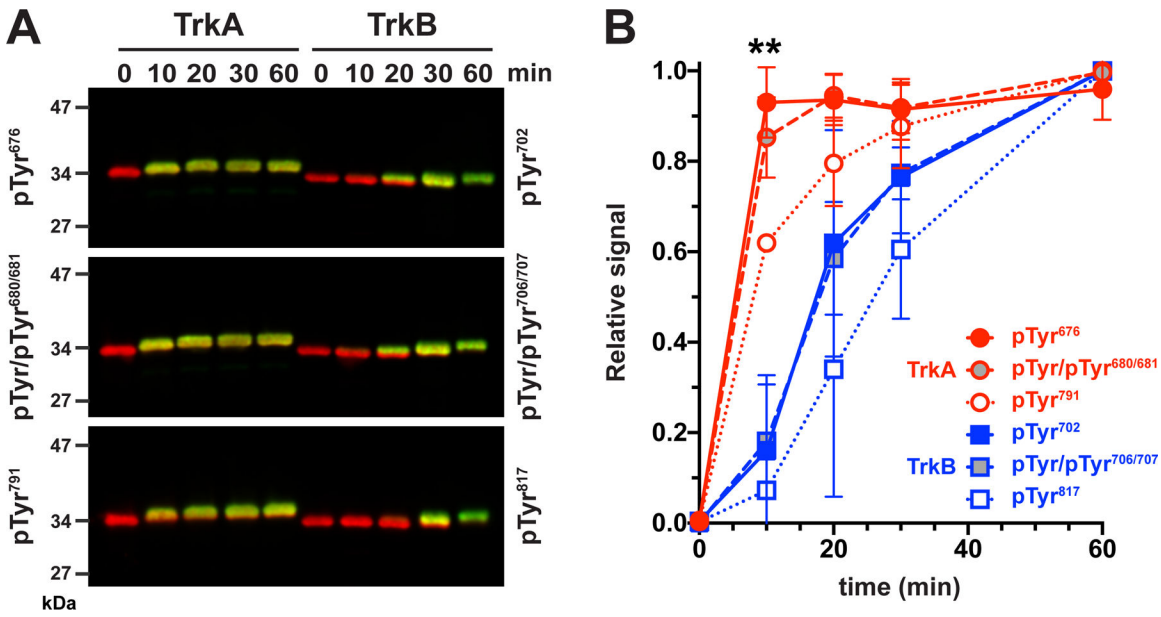

FIGURE 2: Monitoring autophosphorylation of TrkA and TrkB TKDs

Autophosphorylation assays were performed at 15°C with 5 μM TrkA or TrkB TKD in the presence of 1 mM ATP and 10 mM $MgCl_2$ in a buffer containing 100 mM HEPES pH 7.4, 150 mM NaCl, 2 mM DTT and 1x Halt phosphatase cocktail inhibitor. Samples were taken at the indicated times and analyzed by LI-COR immunoblotting with the noted antibodies to detect autophosphorylation (green) at Tyr^{676}(TrkA), Tyr^{702}(TrkB), $Tyr/Tyr^{680/681}$(TrkA), $Tyr/Tyr^{706/707}$(TrkB), and Tyr^{791}(TrkA), Tyr^{817}(TrkB) – as well at total Trk TKD protein levels (red). Representative blots are shown in panel **A**. Relative phosphotyrosine signals in Western blots (green) were determined by first normalizing the maximum signal for each phosphospecific antibody to the total Trk signal (red), and plotting (in panel **B**) the signal at each time as a proportion of the maximum for that site. At least three biological repeats were performed for each experiment. Errors bars are standard deviations. Statistical significance of differences between TrkA and TrkB for each pTyr-specific antibody was determined using the Bonferroni-Dunn method ($\alpha = 0.05$) to correct for multiple comparisons. Significant differences were seen only at the 10 min time point. Adjusted P values (after Bonferroni correction) were $^{**}P < 0.01$.

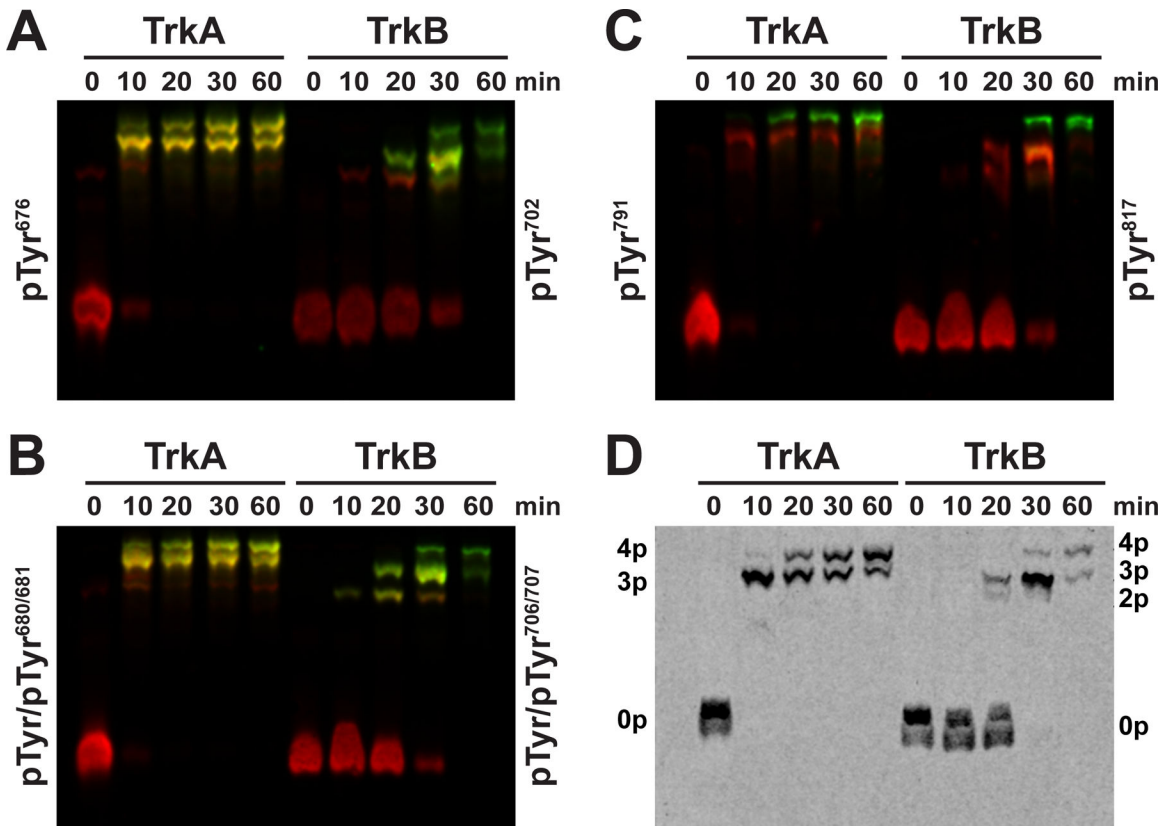

FIGURE 3: Phos-tag comparison of phosphorylation order

Representative Phos-Tag SDS PAGE/Western blots of samples from an autophosphorylation reaction performed as in Fig. 2 are shown, using antibodies against the Trk TKDs (red) or (in green) phosphospecific antibodies that recognize: (**A**) phosphorylated Tyr^{676}(TrkA) or Tyr^{702}(TrkB); (**B**) phosphorylated $Tyr/Tyr^{680/681}$(TrkA) or $Tyr/Tyr^{706/707}$(TrkB); or (**C**) phosphorylated Tyr^{702}(TrkA) or Tyr^{817}(TrkB). In addition, a Coomassie stained Phos-Tag gel of an autophosphorylation reaction is shown (**D**), with different phosphoforms marked as described in the text.

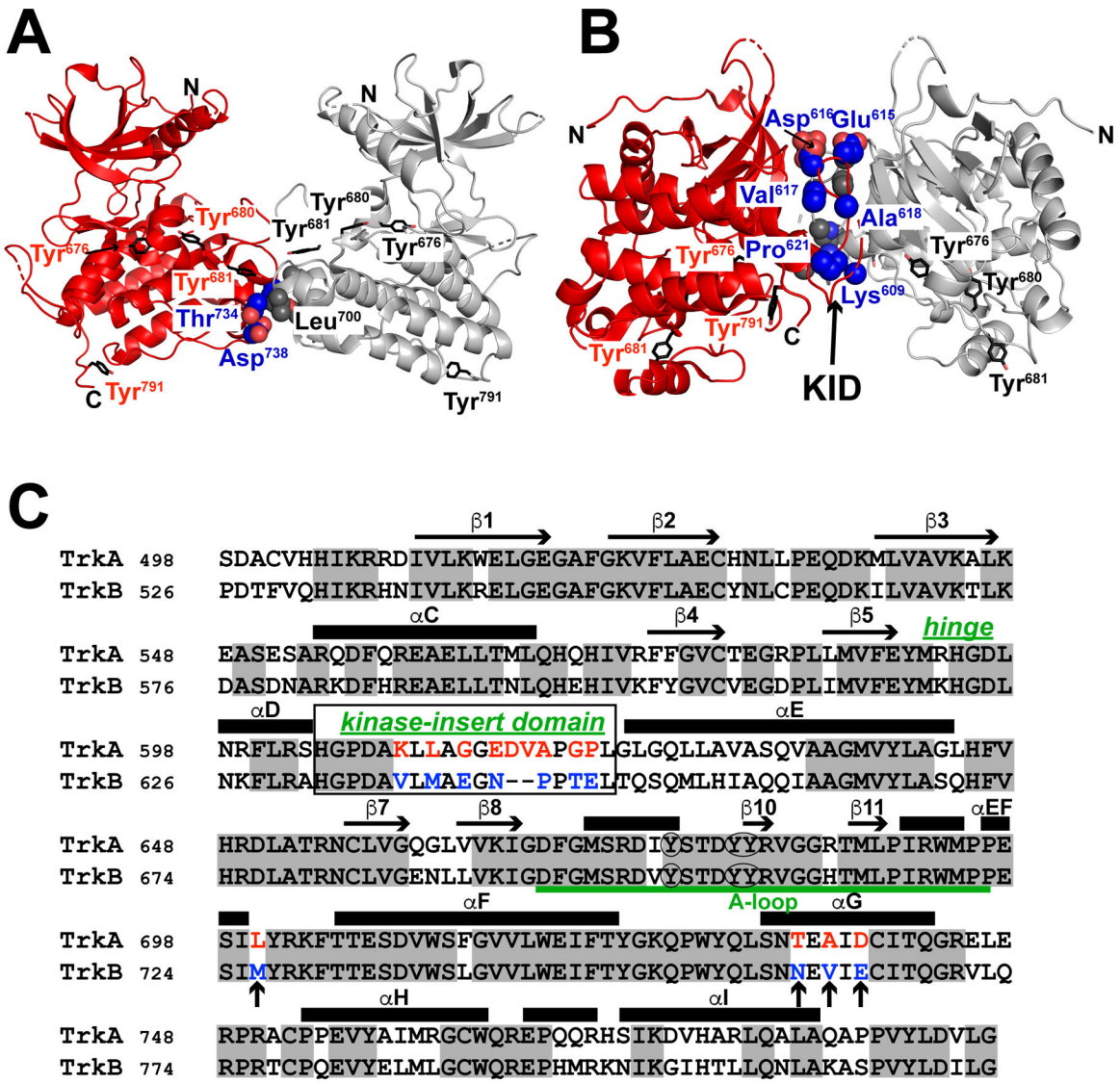

FIGURE 4: TrkA TKD dimers seen in crystal structures

(**A**) The face-to-face TrkA TKD dimer mentioned in the text, seen in 50% of available TrkA TKD crystal structures, shown specifically for PDB ID 4GT5 [25]. Tyrosine autophosphorylation sites are marked where visible in the orientation shown. So are the C-lobe residues that interact across the interface (Leu^{700} between αEF and αF and Thr^{734}/Asp^{738} in αG), which are all different in TrkB.

(**B**) The KID-mediated TrkA TKD dimer described in the text, also seen in 50% of available TrkA TKD crystal structures, shown specifically for PDB ID 4GT5 [25]. Again, tyrosine autophosphorylation sites are marked where visible in the orientation shown. So are the kinase insert domain (KID) residues that interact across the interface: Lys^{609} (Val in TrkB), Glu^{615} (Asn in TrkB), Asp^{616} (deleted in TrkB), Val^{617} (deleted in TrkB), Ala^{618} (Pro in TrkB), and Pro^{621} (Pro in TrkB). The KID is also marked, as are N- and C-termini where visible.

(**C**) Sequence alignment of TrkA and TrkB TKDs, marking regions of sequence identity (share grey), and secondary structure elements as guided by PDB ID 4GT5. The 'hinge' region, kinase-insert domain (KID) and activation loop (A-loop) are labeled with green text. Autophosphorylated tyrosines in the A-loop are circled. Residues that differ in the interfaces shown in **A** (in αEF and αG) and **B** (in the KID) are colored red for TrkA and blue for TrkB. Sequence numbers correspond to those in NCBI reference sequences NM_002529.3 (TrkA) and NM_001018064 (TrkB).

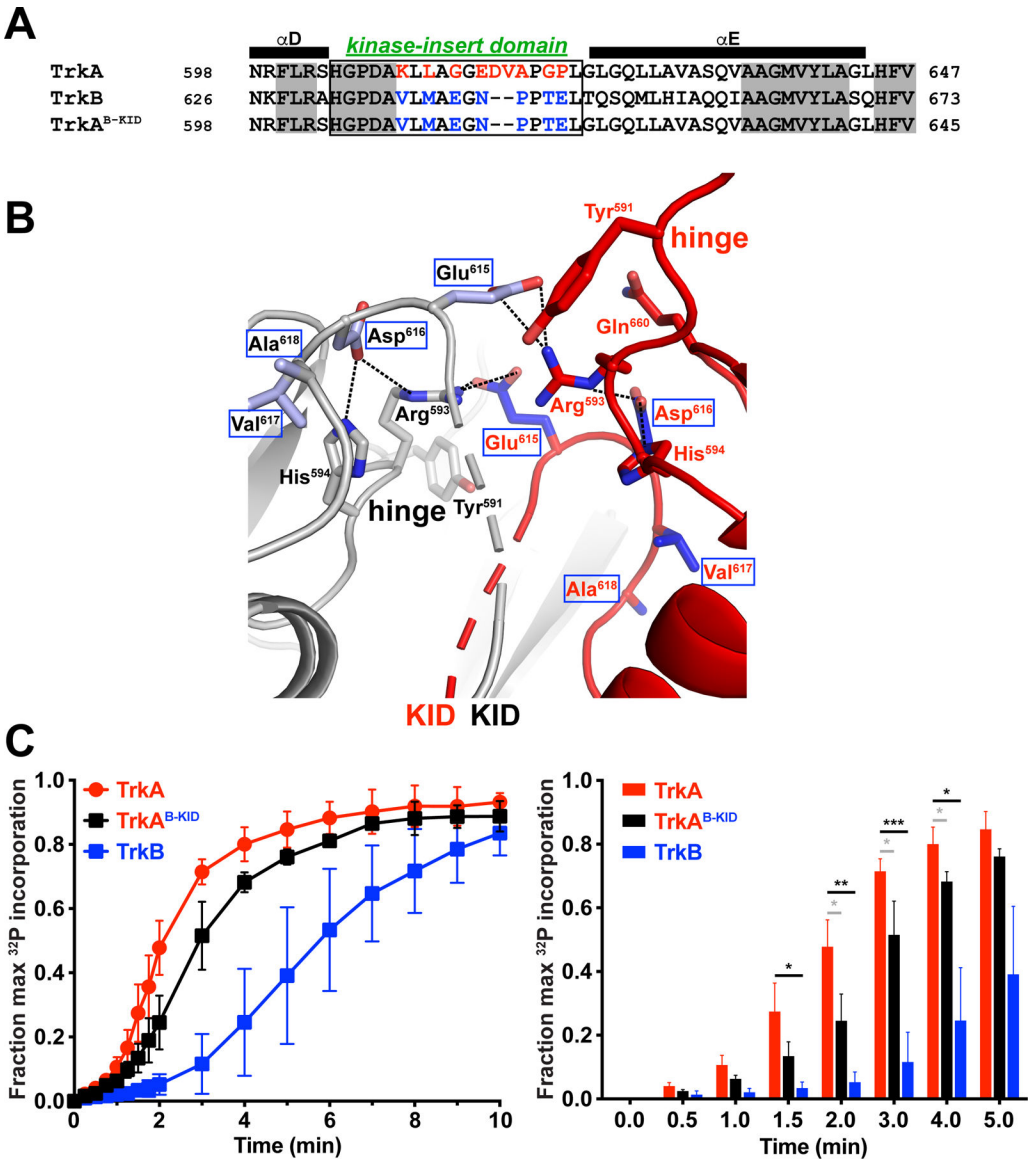

FIGURE 5: Effect of KID mutations on TrkA TKD autophosphorylation

(**A**) Sequence alignment across αD, the KID and αE for the TrkA and TrkB TKDs, depicting the alterations made in this region of TrkA to generate the TrkA$^{B\text{-}KID}$ TKD variant. Colors and labels are as in Fig. 4C.

(**B**) Close-up view of the KID-mediated interactions between the two TrkA TKDs in the crystallographic dimer seen in 4GT5 and half of the subsequently determined TrkA TKD crystal structures. The hinge and KID regions are noted for the two TKDs (colored grey and red). KID residues Glu^{615}, Asp^{616}, Val^{617}, and Ala^{618} are labeled for both molecules – and boxed in blue (these are all different in TrkB). Hinge region residues that also participate in the dimer interaction (and/or intramolecular interactions with the KID) are also shown and labeled. Note the predicted intermolecular polar interactions between Arg^{593} (in the hinge) of one TKD and Glu^{615} (in the KID) of the other. This interaction is set up by intramolecular interactions between Asp^{616} (KID) and Arg^{593} (hinge).

(**C**) Results for radioactive autophosphorylation assays performed at room temperature for 4 μM of TrkA, TrkA$^{B\text{-}KID}$, or TrkB TKDs. The left-hand plot shows progression of autophosphorylation with time over 10 min. The bar graph shown in the right-hand panel compares data points for the three TRKs in the first 5 min. At least 3 biological replicates were performed. As also seen in Fig. 2, TrkA and TrkB TKDs are significantly different at the 1.5 min, 2 min, 3 min, and 4 min time points using the using the Bonferroni-Dunn method ($\alpha = 0.05$) to correct for multiple comparisons, with adjusted P values (after Bonferroni correction) *P < 0.05, **P < 0.01, and ***P < 0.005. Differences between TrkA and TrkA$^{B\text{-}KID}$ were significant (*P < 0.05) at the 2 min, 3 min, and 4 min timepoints without correction for multiple comparisons (see grey asterisks), but lost significance upon Bonferroni correction.

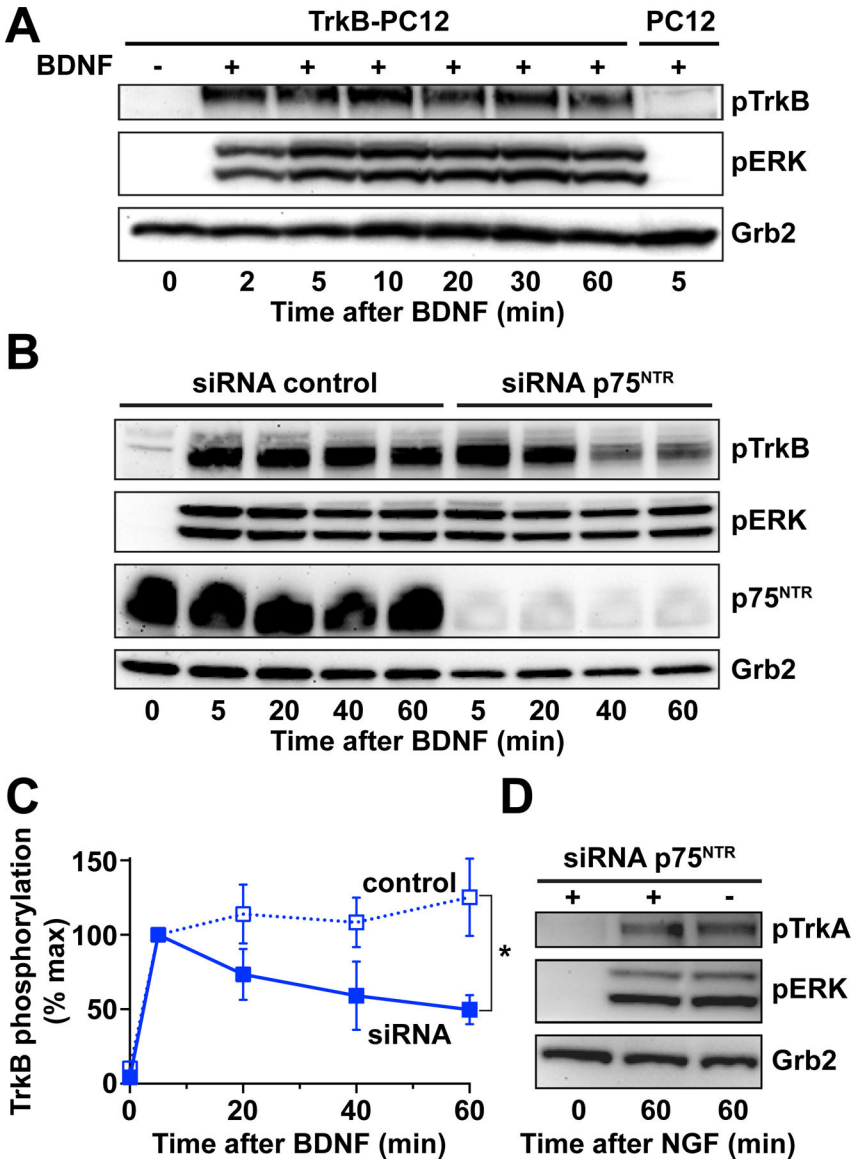

FIGURE 6: TrkB signaling in PC12 cells

(**A**) TrkB signaling was compared in PC12 cells stably expressing TrkB (see Materials and Methods) and parental PC12 cells. Serum-starved TrkB-PC12 or PC12 cells were either left unstimulated or were stimulated with 50 ng/ml BDNF for the indicated times (5 min for parental cells), and phosphorylation of TrkB and ERK1/2 determined by immunoblotting, with Grb2 as a loading control as described [14, 15].

(**B**) TrkB-PC12 cells were transiently transfected with either 100 nM siRNA specific for rat $p75^{NTR}$ (siRNA $p75^{NTR}$) or 100 nM non-targeting negative control (siRNA control). 72 hours following transfection, serum-starved cells were stimulated with 50 ng/ml BDNF for the indicated times. Levels of phosphorylated TrkB ($pTyr^{817}$), phosphorylated ERK1/2 ($pThr^{202}/pTyr^{204}$), as well as total $p75^{NTR}$ and Grb2 (as loading control) were determined by immunoblotting of total cell lysates. Blots representative of 3 independent experiments are shown.

(**C**) Quantitation of pTrkB levels (normalized to Grb2 and the peak value at 5 min) after knockdown of $p75^{NTR}$ (solid blue line) and negative control (dotted blue line) (from **B**), plotting mean ± SD (n = 3 experiments). Statistical significance of the difference between control and $p75^{NTR}$ siRNA samples was assessed using the Bonferroni-Dunn method (α = 0.05) to correct for multiple comparisons, with adjusted P values (after Bonferroni correction) *P < 0.05 for the 60 min time point.

(**D**) Parental PC12 cells (which express TrkA) were transiently transfected with either 100 nM siRNA specific for rat $p75^{NTR}$ (+) or 100 nM non-targeting negative control (−). 72 hours following transfection, serum-starved cells were stimulated with 50 ng/ml NGF for the indicated times. Levels of phosphorylated TrkA, phosphorylated ERK1/2 ($pThr^{202}/pTyr^{204}$), and Grb2 (as loading control) were determined by immunoblotting of total cell lysates. Blots representative of 3 independent experiments are shown.

Table 1.

Summary of kinetic parameters of TrkA and TrkB TKDs in the inactive (dephosphorylated) or active (phosphorylated) states.

Data are shown as mean ± standard deviation of at least 3 experiments. The Mann-Whitney-Wilcoxon test was used to determine statistical significance of differences between TrkA and TrkB. Adjusted P values were *P < 0.05.

kinase	k_{cat} (min^{-1})	$K_{m,\ ATP}$ (mM)	$k_{cat}/K_{m,\ ATP}$ ($min^{-1}\ mM^{-1}$)	$K_{m,\ peptide}$ (mM)	$k_{cat}/K_{m,\ peptide}$ ($min^{-1}\ mM^{-1}$)
TrkA	18.7 ± 3.9	2.09 ± 0.52	9.83 ± 2.50	1.82 ± 0.74	10.4 ± 2.3
TrkB	14.0 ± 6.4	3.20 ± 1.69	5.85 ± 1.94	1.17 ± 0.42	9.40 ± 5.23
pTrkA	1326 ± 297	0.18 ± 0.05	6204 ± 673*	0.35 ± 0.04	4169 ± 434
pTrkB	1201 ± 410	0.29 ± 0.14	3641 ± 423*	0.39 ± 0.06	3815 ± 266